A Developmental Model for Generating Frequency Maps in the Reptilian and Avian Cochleas

Yuh-Cherng Wu and Robert Fettiplace
Department of Neurophysiology, University of Wisconsin Medical School, Madison, Wisconsin 53706 USA

ABSTRACT Hair cells in the turtle cochlea are frequency-tuned by a mechanism involving the combined activation of voltage-sensitive Ca^{2+} channels and Ca^{2+}-activated K^+ (K_{Ca}) channels. The main determinants of a hair cell's characteristic frequency (F_o) are the K_{Ca} channels' density and kinetics, both of which change systematically with location in the cochlea in conjunction with the observed frequency map. We have developed a model based on the differential expression of two K_{Ca} channel subunits, which when accompanied by concurrent changes in other properties (e.g., density of Ca^{2+} channels and inwardly rectifying K^+ channels), will generate sharp tuning at frequencies from 40 to 600 Hz. The kinetic properties of the two subunits were derived from previous single-channel analysis, and it was assumed that the subunits (A and B) combine to form five species of tetrameric channel (A_4, A_3B, A_2B_2, AB_3, and B_4) with intermediate kinetics and overlapping distribution. Expression of K_{Ca} and other channels was assumed to be regulated by diffusional gradients in either one or two chemicals. The results are consistent with both current- and voltage-clamp data on turtle hair cells, and they show that five channel species are sufficient to produce smooth changes in both F_o and kinetics of the macroscopic K_{Ca} current. Other schemes for varying K_{Ca} channel kinetics are examined, including one that allows extension of the model to the chick cochlea to produce hair cells with F_o's from 130 to 4000 Hz. A necessary assumption in all models is a gradient in the values of the parameters identified with the cell's cytoplasmic Ca^{2+} buffer.

INTRODUCTION

The speed and sensitivity of many sensory receptors are inversely related, with a receptor achieving high sensitivity only at the expense of temporal resolution. One reason for this interdependence stems from the relationship between input resistance and the time constant for a membrane that behaves like a low-pass filter. Thus for a brief transducer current, the higher the input resistance the larger but slower the receptor potential. This limitation has been circumvented in the cochleas of lower vertebrates, where the hair cells have acquired an electrical tuning mechanism in which the membrane behaves like a sharply tuned resonance (Crawford and Fettiplace, 1981; Fettiplace, 1987). The resonance maximizes the membrane impedance, and hence sensitivity, over a small range of frequencies around the resonant frequency, F_o, and for a wide-band transducer current, the amplitude of the receptor potential is largest at F_o. To expand the organ's frequency range, different receptor cells possess different resonant frequencies smoothly covering the frequency domain, which in the turtle's cochlea extends from about 40 Hz to 600 Hz (Crawford and Fettiplace, 1980).

Electrical tuning occurs in hair cells of turtle (Crawford and Fettiplace, 1981), frog (Hudspeth and Lewis, 1988a,b; Pitchford and Ashmore, 1987), chick (Fuchs et al., 1988), alligator (Fuchs and Evans, 1988), and goldfish (Sugihara and Furukawa, 1989). In all cases the dominant mechanism involves combined activation of voltage-sensitive Ca^{2+} channels and Ca^{2+}-activated K^+ (K_{Ca}) channels (Fuchs, 1992). In the turtle cochlea, the hair cell's resonant frequency is most closely allied with the density and kinetics of the K_{Ca} channels (Art and Fettiplace, 1987; Wu et al., 1995), but there are concurrent variations in the complement of Ca^{2+} channels (Art et al., 1993) and inwardly rectifying K^+ channels (Goodman and Art, 1996) and in the morphology of the hair bundle (Hackney et al., 1993). The resonant frequency changes systematically with the hair cell's location in the cochlea (Crawford and Fettiplace, 1980), implying that there must be gradients in cellular properties along the cochlear epithelium. The mechanisms that guide the development of such gradients are unknown, although modeling indicates (Wu et al., 1995) that the various channel profiles must be closely matched to produce sharp tuning at the appropriate frequency. It may therefore be most economical for a single process to coordinate the diversity in the different channel types.

A key to understanding this developmental question may be the regulation of the large-conductance K_{Ca} channels. How many types of K_{Ca} channel protein are required to make the map? If this number is large, then it is more likely that a single channel protein is subject to modulation, but if the number is small, then an alternative explanation would be that a few different gene transcripts can generate the distribution. A conclusion from earlier modeling (Wu et al., 1995) was that although the K_{Ca} channel kinetics was the major determinant of F_o, the number of K_{Ca} channels needed to fall within a restricted range to produce sharp tuning. How might these two channel parameters be coregulated? With the recent cloning of the Ca^{2+}-activated K^+

Received for publication 21 December 1995 and in final form 27 February 1996.

Address reprint requests to Dr. Robert Fettiplace, 273 Medical Sciences Building, 1300 University Avenue, Madison, WI 53706. Tel.: 608-262-9320; Fax: 608-265-3500; E-mail: fettiplace@neurophys.wise.edu.

0006-3495/96/06/2557/14 $2.00

channel, it is clear that there are several sites for alternative RNA splicing of a single transcript, and the potential for production of channel proteins with diverse kinetic and Ca^{2+} binding properties (Adelman et al., 1992; Butler et al., 1993; Tseng-Crank et al, 1994). The purpose of the present work was to extend our earlier model of electrical tuning by exploring schemes for the joint control of the K_{Ca} channel kinetics and density. Such models may point to possible developmental mechanisms and could provide a rational basis for the search for cochlear K_{Ca} channel clones (Jiang et al., 1995).

THEORY AND RESULTS

Variations in channel density observed experimentally

A majority of the cochlear hair cells in the adult turtle are located on the basilar membrane and organized in roughly 100 rows spanning a length of 750 μm. Measurements on the intact cochlea have shown that hair cells on the basilar membrane possess a resonant frequency, F_o, distributed between 40 Hz and 600 Hz, which is mapped exponentially with distance from the apical end of the organ (Crawford and Fettiplace, 1980; Art et al., 1986). The relationship between F_o and n, the number of rows from the apex, will be described by

$$F_o(n) = F_o(n_{min}) \cdot e^{(n-n_{min})/\lambda}, \quad (1)$$

where n ranges from $n_{min} = 0$ to $n_{max} = 100$, $F_o(n_{min})$ is equal to 40 Hz, and λ is a space constant of 37 rows. Equation 1 was obtained from the exponential frequency map, assuming that the dimensions and packing of the hair cells were constant along the cochlea. Only those hair cells that employ a tuning mechanism involving the K_{Ca} channels will be considered (Wu et al., 1995). The turtle cochlea also includes a category of hair cells, tuned to lower frequencies from 10 Hz to 30 Hz, in which the role of the K_{Ca} channels has been supplanted by voltage-sensitive K^+ channels (Art et al., 1993). Most of these cells are probably confined to the rows overlying the apical limbus ($n < n_{min}$), and they will be excluded from the subsequent analysis.

As previously documented (Art and Fettiplace, 1987; Hudspeth and Lewis, 1988a,b; Wu et al., 1995), four types of membrane channel influence the hair cell's electrical resonance (Fig. 1): i) Voltage-dependent Ca^{2+} (Ca_V) channels open in response to depolarizations positive to −55 mV. ii) K_{Ca} channels are gated by both the change in membrane potential and the consequent elevation in intracellular Ca^{2+}. The K^+ current provides negative feedback control of the membrane potential that generates the resonance. iii) Inwardly rectifying K^+ (K_{IR}) channels are blocked by depolarization, which causes a negative slope in the limb of the K_{IR} current-voltage curve positive to the K^+ equilibrium potential. Thus depolarization produces a reduction in outward current that can contribute to the resting potential and sharpen the resonance. iv) Mechanoelectrical

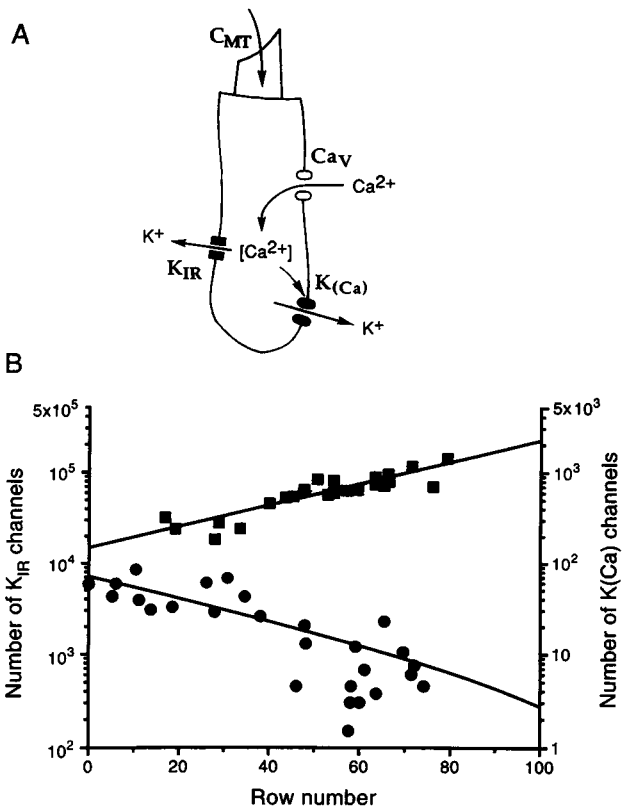

FIGURE 1 (*A*) Schematic turtle hair cell showing the membrane channels that contribute to transduction and tuning. C_{MT}, the cation-selective mechano-transducer channels in the hair bundle; Ca_V, voltage-dependent L-type Ca^{2+} channels; K_{Ca}, large-conductance Ca^{2+}-activated K^+ channels; K_{IR}, inwardly rectifying K^+ channels. (*B*) Variations in the numbers of K_{Ca} channels (■) and K_{IR} channels (●) with hair cell row number from the apical end of the turtle basilar papilla. Values based on measurements of conductances in isolated hair cells for the K_{Ca} channels (taken from Art et al., 1993) and for the K_{IR} channels (taken with permission from Goodman, 1995). Lines calculated from Eqs. 2 and 3.

transduction (C_{MT}) channels contribute a voltage-independent leak conductance, which damps the resonance. The equations that describe the kinetics and voltage dependences of these conductances, collected in the Appendix, were derived from measurements on enzymatically isolated hair cells (Wu et al., 1995). To a first approximation, the number and kinetics of the K_{Ca} channels dictate the resonant frequency, whereas the other three channel types contribute to the sharpness of tuning. The abundance of each of these channels in hair cells varies along the length of the basilar membrane (Wu et al., 1995; Goodman and Art, 1996), the densities of the K_{Ca}, Ca_V, and C_{MT} channels increasing and the density of the K_{IR} channels decreasing with resonant frequency. The mappings of the numbers of K_{Ca} and K_{IR} channels are shown in Fig. 1 *B* and can be described by

$$N_{KCa}(n) = a_F \cdot F_o(n) = a_F \cdot F_o(n_{min}) \cdot e^{(n-n_{min})/\lambda}, \quad (2)$$

$$N_{K_{IR}}(n) = a_o + a_1 \cdot e^{(n_{min}-n)/\lambda}, \quad (3)$$

where $a_F = 3.75$, $a_o = -221$, and $a_1 = 7370$. The numbers of K_{IR} channels were inferred from the conductance data in

Goodman (1995), scaled by a unitary conductance of 4 pS (Sackmann and Trube, 1984). The Ca^{2+} channels are also mapped, there being approximately twice as many Ca^{2+} channels in a given cell as K_{Ca} channels (Art et al., 1993),

$$N_{Ca}(n) = 2 \cdot N_{KCa}(n). \quad (4)$$

Overwhelming evidence indicates that the mechanoelectrical transduction channels are placed at the ends of the tip links that connect adjacent stereocilia (Pickles and Corey, 1992). The number of transducer channels should therefore be proportional to the number of stereocilia in the hair bundle, which in all cochleas increases from the low-frequency to the high-frequency end (e.g., Tilney and Saunders, 1983). The leak conductance, G_L, stems partly from the resting probability of opening of the transducer channels. Although there is no direct evidence for systematic differences in transducer conductance, the leak conductance, G_L in pS, will be assumed to increase along the cochlea in parallel with the change in stereociliary complement, given in pS as a function of row number by

$$G_L(n) = 2181.82 + 254.54 \cdot e^{n/\lambda}. \quad (5)$$

Equation 5 produces a 2.4-fold increase in leak conductance from the low-frequency to the high-frequency end of the cochlea. Apart from the four membrane conductances, one other variable of the model needs specifying. This is the relationship between the average single Ca^{2+} channel current, $\bar{i}_{Ca}$ (see Appendix), and the intracellular Ca^{2+} concentration, $[Ca^{2+}]$, at the mouth of the K_{Ca} channel. A simple description is provided by the first-order differential equation (Wu et al., 1995)

$$\frac{d[Ca^{2+}]}{dt} = S_f \cdot \bar{i}_{Ca} - k_R \cdot [Ca^{2+}], \quad (6)$$

where k_R (in ms^{-1}) is a removal rate constant and S_f (in $\mu M/ms/nA$) is a scaling factor, which together determine the time course and steady level of the Ca^{2+} concentration change. These two constants embody the intracellular handling of Ca^{2+}, its buffering and extrusion, which may likely vary along the cochlea to match the change in the amplitude of the Ca^{2+} current. In our previous modeling (Wu et al., 1995) it was necessary to make S_f increase with F_0 to raise the Ca^{2+} concentration high enough locally to activate the K_{Ca} channel. In the present analysis alterations in k_R, the removal rate, were also allowed to optimize the tuning. Both S_f and k_R then become empirically derived functions of the row number (see Appendix).

Equations 2 through 5 define the variations in channel numbers, and having a similar form, they might represent a gradient in the concentration of a single regulator molecule, X, distributed exponentially along the cochlea. Three of the conductances, K_{Ca}, Ca_V, and C_{MT}, increase with X, whereas the fourth, K_{IR}, decreases; i.e., X inhibits the production of K_{IR} channels. If the regulator is regarded solely as an activating molecule, then opposing gradients in two separate regulators, Y and Z, are needed. A scheme using two such regulators will also be considered.

K_{Ca} channel kinetics

The main factor dictating the resonant frequency is the kinetic behavior of the K_{Ca} channels (Art and Fettiplace, 1987), which have been characterized in inside-out patches of membrane from hair cells of known resonant frequency (Art et al., 1995). In those patches containing a single channel, a range of mean open time from about 0.4 to 13 ms was observed. To include multichannel patches, the relaxation time constant of the ensemble current at −50 mV in 4 μM Ca^{2+} was employed as a measure of the channel kinetics. Fig. 2 *A* shows the correlation of this time constant with resonant frequency, the measurements spanning a range similar to that of the open times. The data are likely to be incomplete at the high-frequency end, where cells are found with resonant frequencies in vivo extending up to 600 Hz (Crawford and Fettiplace, 1980). Although there is little clear evidence of the groupings corresponding to distinguishable channel types, this might be obscured by slight variations in experimental conditions or inaccuracies in fitting the relaxation time constants.

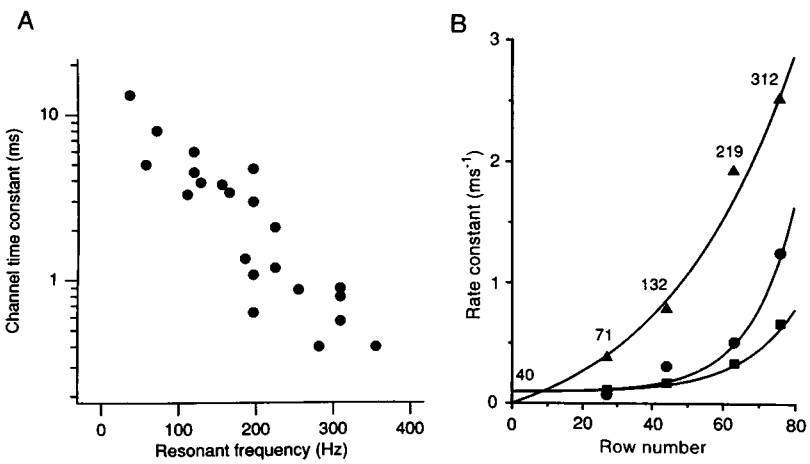

FIGURE 2 (*A*) K_{Ca} channel time constants obtained by fitting the relaxation in the average single-channel current at −50 mV in 4 μM Ca^{2+} on the inside face of the membrane patches (Art et al., 1995). Resonant frequency of isolated hair cell inferred from height of hair bundle. (*B*) Variations in the rate constants in the K_{Ca} channel kinetic scheme, Eq. 7 deduced from fitting dwell-time distributions (Wu et al., 1995). $C_{1Ca} \rightarrow C_{2Ca}$ (■) and $C_{3Ca} \rightarrow C_{4Ca}$ (●) are the forward rate constants for binding the second and fourth Ca^{2+} atoms, both evaluated at −50 mV and 10 μM Ca^{2+}; $O_{4Ca} \rightarrow C_{4Ca}$ (▲) is the final closing transition. Smooth curves are fits calculated from Eqs. A13, A14, and A15. The resonant frequencies (71, 132, 219, and 312 Hz) corresponding to the four sets of measurements are given above the points. Row 0 is at 40 Hz.

Reconstruction of electrical resonance requires specification of a kinetic scheme for the K_{Ca} channels coupled with a procedure for varying the scheme with the resonant frequency. The scheme and sets of rate constants were taken from previous analysis of single-channel measurements, which involved fitting open- and closed-time histograms over a wide range of membrane potentials and Ca^{2+} concentrations (Wu et al., 1995). The kinetic scheme used resembled one of the set examined by McManus and Magleby (1991):

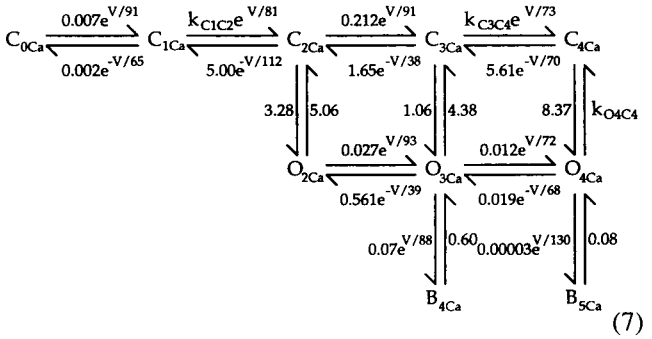

(7)

where C_{iCa}, O_{iCa}, and B_{iCa} refer to closed, open, and blocked states of the channel, respectively, with i Ca^{2+} ions bound; V is membrane potential (in mV); and rate constants are in $\mu M^{-1}ms^{-1}$ or ms^{-1}. The Ca^{2+} binding and unbinding steps, but not the opening and closing steps, must be voltage sensitive. We previously found that channels with different kinetics could all be fit by a common scheme in which only three of the rate constants varied systematically. Those were the rate constants for binding of the second and fourth Ca^{2+} ions ($C_{1Ca} \rightarrow C_{2Ca}$ and $C_{3Ca} \rightarrow C_{4Ca}$), and the final closing rate constant ($O_{4Ca} \rightarrow C_{4Ca}$), which largely determines the mean open time. The values of these rate constants are plotted in Fig. 2 *B* as a function of row number, inferred from the resonant frequency (71, 132, 219, and 312 Hz). The rate constants have been evaluated at a membrane potential of −50 mV and an intracellular Ca^{2+} concentration of 10 μM. The smooth curves are exponential fits that will be used to extract the kinetics of the individual channel types (see below).

Single-regulator case of K_{Ca} channels

Each K_{Ca} channel is assumed, by analogy with *Shaker* K^+ channels (Isacoff et al., 1990; MacKinnon, 1991), to consist of four subunits. Let S represent one subunit of the channel, S being derived from two independent sources, denoted as A and B (Fig. 3). The assembly of four subunits into a K_{Ca} channel can be described by

$$4[S] \underset{k_{-1}}{\overset{k_1}{\leftrightarrow}} [S_4] \underset{k_{-2}}{\overset{k_2}{\leftrightarrow}} \frac{S_4}{V_{cell}}, \tag{8}$$

where [S] is the sum of concentrations A and B (in μM), $[S_4]$ is the concentration of a transitional state formed from

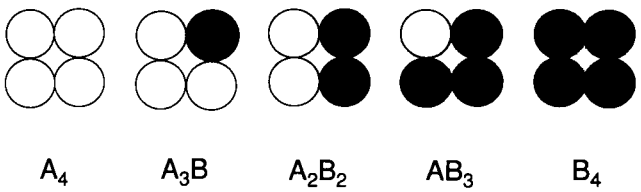

FIGURE 3 The five channel types that can be generated by incorporation of two different subunits (*A, open circles* and *B, filled circles*) into a tetrameric K_{Ca} channel. A tetramer for the K_{Ca} channel is assumed by analogy with voltage-dependent K^+ channels.

the four subunits (in μM), S_4 (in μmol) is the total quantity of K_{Ca} channels located in the membrane, V_{cell} (in liters) is the volume of the hair cell, k_1 (in ms^{-1} μM^{-3}) and k_{-1} (in ms^{-1}) describe the forward and backward rate constants for the integration of the subunits, and k_2 and k_{-2} (in ms^{-1}) are the lumped forward and backward rate constants for the channel's insertion. The differential equations that describe these reactions can be written as follows:

$$\frac{d[S]}{dt} = k_{-1}[S_4] - k_1[S]^4, \tag{9}$$

$$\frac{dS_4}{dt} = k_2[S_4] - k_{-2}\frac{S_4}{V_{cell}}. \tag{10}$$

Then, the steady-state concentration $[S]_n^\infty$ of the hair cell located at the nth row from the apex can be expressed in terms of the rate constants, k_1, k_{-1}, k_2, and k_{-2}; the cell volume, V_{cell}; and the total number of K_{Ca} channels, $N_{KCa}(n) = S_4 \cdot M_o$,

$$[S]_n^\infty = [A]_n^\infty + [B]_n^\infty = \sqrt[4]{\frac{k_{-1} \cdot k_{-2} \cdot N_{KCa}(n)}{k_1 \cdot k_2 \cdot M_o \cdot V_{cell}}}, \tag{11}$$

where M_o, Avogadro's number, is $6.02 \times 10^{17}/\mu$mol. Two experimentally determined relationships introduced above are used to define the steady-state concentration $[S]_n^\infty$ as a function of the location of the hair cell. Using Eqs. 1 and 2, Eq. 11 can be specified in terms of the cell's location in the nth row:

$$[S]_n^\infty = [A]_n^\infty + [B]_n^\infty \tag{12}$$

$$= \sqrt[4]{\frac{k_{-1} \cdot k_{-2} \cdot a_F \cdot F_o(n_{min})}{k_1 \cdot k_2 \cdot M_o \cdot V_{cell} \cdot e^{n_{min}/\lambda}}} \cdot e^{n/4\lambda} = \omega \cdot e^{n/4\lambda},$$

where ω is a constant representing the terms involving the fourth root. ω will serve as a scaling constant that determines the absolute value of $[A]_n^\infty$ and $[B]_n^\infty$, but has no effect on either the gradient of the subunit concentrations or the total number of channels.

For the simplest analysis, the concentration $[S]_n^\infty$ is assumed to be regulated by a gradient in a single regulator molecule, X, with concentration in μM, $[X]_n^\infty$, that varies exponentially along the cochlea:

$$[X]_n^\infty = [X_o] \cdot e^{n/\lambda}, \tag{13}$$

where $[X_o]$ is a fixed concentration (in μM). With the exponential profile, the steady-state concentrations of $[A]_n^\infty$ and $[B]_n^\infty$ can be related to $[X]_n^\infty$, but the connecting function is undetermined. As a simple approach, a power function will be used:

$$[A]_n^\infty = C_A + \gamma_A \cdot ([X]_n^\infty)^{m_A}, \tag{14}$$

$$[B]_n^\infty = C_B + \gamma_B \cdot ([X]_n^\infty)^{m_B}, \tag{15}$$

where C_A, γ_A, m_A, C_B, γ_B, and m_B are parameters to be determined. The boundary conditions described in Eqs. 16 and 17, in addition to Eq. 12, provide three criteria for identifying the values of those parameters:

$$[A]_{n_{min}}^\infty = [A_o], [B]_{n_{min}}^\infty = 0\ \mu M \quad \text{for } n = n_{min}, \tag{16}$$

$$[B]_{n_{max}}^\infty = [B_o], [A]_{n_{max}}^\infty = 0\ \mu M, \quad \text{for } n = n_{max}. \tag{17}$$

Based on the three constraints, the parameters in Eqs. 14 and 15 can be computed as

$$m_A = m_B = 1/4, \tag{18}$$

$$[A_o] = \omega \cdot e^{n_{min}/4\lambda} = [B_o] \cdot e^{(n_{min}-n_{max})/4\lambda}, \tag{19}$$

$$[B_o] = \omega \cdot e^{n_{max}/4\lambda} = [A_o] \cdot e^{(n_{max}-n_{min})/4\lambda}, \tag{20}$$

$$\gamma_A = \frac{[A_o]}{\sqrt[4]{[X_o]} \cdot (e^{n_{min}/4\lambda} - e^{n_{max}/4\lambda})}, \tag{21}$$

$$\gamma_B = \frac{[B_o]}{\sqrt[4]{[X_o]} \cdot (e^{n_{max}/4\lambda} - e^{n_{min}/4\lambda})}, \tag{22}$$

$$C_A = \frac{[A_o]}{1 - e^{(n_{min}-n_{max})/4\lambda}}, \tag{23}$$

$$C_B = \frac{[B_o]}{1 - e^{(n_{max}-n_{min})/4\lambda}}. \tag{24}$$

By substituting Eqs. 18 to 24 into Eqs. 14 and 15, the relationships between $[A]_n^\infty$, $[B]_n^\infty$, and $[X]_n^\infty$ then can be identified as

$$\begin{aligned}[A]_n^\infty &= \omega \cdot e^{n_{min}/4\lambda} \cdot \frac{(e^{n_{max}/4\lambda} - e^{n/4\lambda})}{(e^{n_{max}/4\lambda} - e^{n_{min}/4\lambda})} \\ &= \omega \cdot e^{n_{min}/4\lambda} \cdot \frac{(e^{n_{max}/4\lambda} - \sqrt[4]{[X]_n^\infty/[X_o]})}{(e^{n_{max}/4\lambda} - e^{n_{min}/4\lambda})},\end{aligned} \tag{25}$$

$$\begin{aligned}[B]_n^\infty &= \omega \cdot e^{n_{max}/4\lambda} \cdot \frac{(e^{n/4\lambda} - e^{n_{min}/4\lambda})}{(e^{n_{max}/4\lambda} - e^{n_{min}/4\lambda})} \\ &= \omega \cdot e^{n_{max}/4\lambda} \cdot \frac{(\sqrt[4]{[X]_n^\infty/[X_o]} - e^{n_{min}/4\lambda})}{(e^{n_{max}/4\lambda} - e^{n_{min}/4\lambda})}.\end{aligned} \tag{26}$$

Note that $[A]_n^\infty$ and $[B]_n^\infty$ can be computed directly from the location of the hair cell without knowing the absolute value of $[X_o]$. The normalized concentrations of the two subunits, $[A]_n^\infty/\omega$ and $[B]_n^\infty/\omega$, are given as functions of row number in Fig. 4 *A*. From Eq. 11, the total number of K_{Ca} channels in the hair cell located in the nth row can be derived from the concentrations $[A]_n^\infty$ and $[B]_n^\infty$. Furthermore, if each subunit is either A or B, there will be five combinations of A and B to form a K_{Ca} channel, i.e., A_4, A_3B_1, A_2B_2, A_1B_3, and B_4 (Fig. 3). The five types of multimeric channels presumably have different kinetic schemes, and the hybrid composition of the five types of channels will allow hair cells to be tuned to different frequencies. Because the concentrations $[A]_n^\infty$ and $[B]_n^\infty$ are assumed to be independent of each other, by substituting Eqs. 25 and 26 into Eq. 11 and expanding the fourth-order polynomial, the number of each type of channel can be described as follows:

$$\begin{aligned}N_{A_pB_q} &= \frac{(p+q)! \cdot k_1 \cdot k_2 \cdot M_o \cdot V_{cell}}{p! \cdot q! \cdot k_{-1} \cdot k_{-2}} \\ &\quad \cdot ([A]_n^\infty)^p \cdot ([B]_n^\infty)^q \\ &= \frac{(p+q)! \cdot a_F \cdot F_o(n_{min}) \cdot e^{(p \cdot n_{min} + q \cdot n_{max})/4\lambda}}{p! \cdot q! \cdot (e^{n_{max}/4\lambda} - e^{n_{min}/4\lambda})^4 \cdot e^{n_{min}/\lambda}} \\ &\quad \cdot (e^{n_{max}/4\lambda} - e^{n/4\lambda})^p \cdot (e^{n/4\lambda} - e^{n_{min}/4\lambda})^q \\ &= \frac{(p+q)! \cdot a_F \cdot F_o(n_{min}) \cdot e^{(p \cdot n_{min} + q \cdot n_{max})/4\lambda}}{p! \cdot q! \cdot (e^{n_{max}/4\lambda} - e^{n_{min}/4\lambda})^4 \cdot e^{n_{min}/\lambda}} \\ &\quad \cdot \left(e^{n_{max}/4\lambda} - \sqrt[4]{\frac{[X]_n^s}{[X_o]}}\right)^p \cdot \left(\sqrt[4]{\frac{[X]_n^s}{[X_o]}} - e^{n_{min}/4\lambda}\right)^q \\ &= \frac{(p+q)! \cdot a_F \cdot F_o(n_{min})}{p! \cdot q! \cdot (1 - e^{(n_{min}-n_{max})/4\lambda})^4} \\ &\quad \cdot \left(1 - \sqrt[4]{\frac{[X]_n^\infty}{[X_o]}} \cdot e^{-n_{max}/4\lambda}\right)^p \cdot \left(\sqrt[4]{\frac{[X]_n^\infty}{[X_o]}} \cdot e^{-n_{min}/4\lambda} - 1\right)^q,\end{aligned} \tag{27}$$

where p and q are integers from 0 to 4, and the sum of p and q is equal to 4. Equation 27 can be employed to determine the kinetics of the five channel types by correlating the variation of three major rate constants (Fig. 2 *B*) and the location of the dominant types of channel. If the numbers of the five types of channels are plotted against the hair cell's location, i.e., its row number n, each type of channel will predominate at a particular location. At any given position the sum of the components yields the total number of K_{Ca} channels, which from experiments increases exponentially with distance from the apex. Fig. 4 *B* shows the distributions of the five channel species along the cochlea. A given channel type may be considered dominant at a position where its probability of occurrence is maximum relative to the sum of the two next most prevalent components. From Fig. 4 *B*, the row index and the corresponding resonant frequency are 0 (40.0 Hz), 23 (74.5 Hz), 42 (124.5 Hz), 63 (219.6 Hz), and 100 (599.8 Hz) for N_{A_4}, $N_{A_3B_1}$, $N_{A_2B_2}$, $N_{A_1B_3}$,

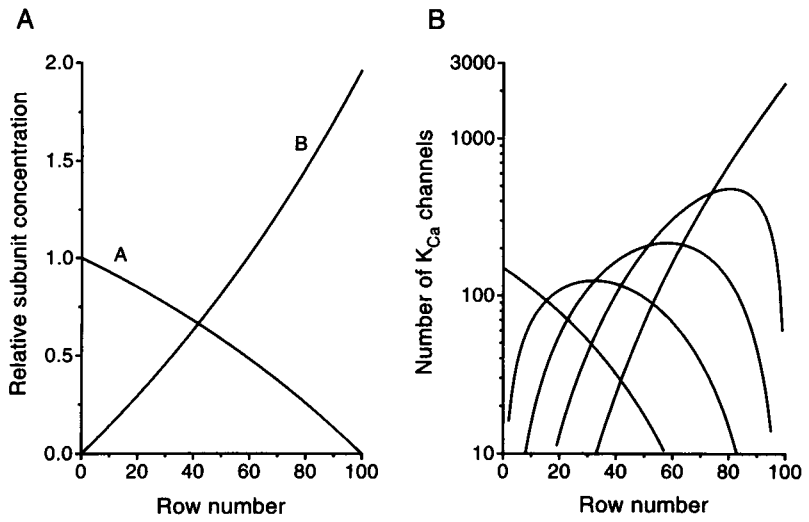

FIGURE 4 (*A*) Theoretical gradients in the normalized concentrations of the A and B subunits of the K_{Ca} channel, $[A]_n^\infty/\omega$ and $[B]_n^\infty/\omega$, with hair cell row number. (*B*) Theoretical distributions of the channel types resulting from the five combinations of the A and B subunits, calculated from Eq. 27.

and N_{B_4} to be the dominant type, respectively. The relative probability of the dominant component for these five locations was 1.0, 0.45, 0.43, 0.45, and 1.0, respectively. A channel formed from two kinetically distinct subunits may have intermediate properties, but at present those properties are not easily predictable (Li et al., 1992). Therefore as an approximation, the three rate constants corresponding to these five locations were interpolated from the single-channel data of Fig. 2 *B* to describe the kinetics for the five types of channel.

Predictions of electrical resonance

The electrical tuning characteristics of model hair cells were predicted from the responses to injected current steps causing small voltage deviations from the resting potential. For a given location, the numbers of all channel types (including the relative proportions of the different subspecies of K_{Ca} channel) were fixed, along with the kinetics of each channel type. As discussed below, the kinetics of Ca^{2+} buffering and extrusion (Eq. 6), for which there are no experimental data, were allowed to vary to optimize tuning. The reconstruction was performed for every fifth row of cells ($n = 5 \cdot j$, where $1 \leq j \leq 20$) by inserting the channel densities and K_{Ca} channel kinetics into the equations for the equivalent electrical circuit, as given in the Appendix. Both the K_{Ca} kinetics stemming from the mixture of the five channel types and the various channel densities were functions of n, as described above. The kinetics of the Ca_V and the K_{IR} channels were established from previous experimental measurements (Wu et al., 1995). The resonant frequency of a given model cell was calculated from the frequency of membrane potential oscillations for current steps from the resting potential, and the quality factor, Q, of the resonance was inferred from the time constant of decay of these oscillations (Crawford and Fettiplace, 1981). Examples of the model responses for rows 25, 50, 75, and 100, having resonant frequencies of 80, 155, 313, and 600 Hz, are shown in Fig. 5 *A*. A maximum quality factor, ranging between 6 and 50, occurred at a membrane potential within 4 mV of the resting potential, which itself varied from −45 to −58 mV. Cells tuned to higher frequencies tended to have more hyperpolarized resting potentials. Nevertheless, all values for the Q and resting potential lay within the range of experimental measurements obtained in the intact turtle cochlea (Crawford and Fettiplace, 1980). The inferred tonotopic map is shown in Fig. 6 *A*, with the change in resonant frequency with row number being well fit by the starting assumption (Eq. 1). It should be noted, however, that such close agreement was not obligatory, and in other forms of the model discussed below the predicted map was not accurately exponential.

The voltage-clamp behavior of the model was also examined by subjecting the cell to 5-mV steps from −50 to −45 mV. To quantify the kinetics of the macroscopic K_{Ca} current, the time course of the current relaxation on repolarization back to −50 mV was measured (Fig. 5 *B*). In agreement with experimental observations (Art and Fettiplace, 1987), the decline in current became faster for higher resonant frequencies. The time course could be reasonably well fit with a single exponential, giving a time constant, τ, that decreased monotonically from 24 ms in the apical row ($n = 0$) to 0.53 ms in the most basal row ($n = 100$). The range of time constants can be displayed by plotting $\tau^{-1/2}$, which increases in proportion to the resonant frequency (Fig. 6 *B*). This feature of the model closely matches the experimental observations (Art and Fettiplace, 1987). Owing to its relatively weak voltage sensitivity, measuring the time constant at the variable resting potential rather than at a fixed potential of −50 mV did not significantly alter the results.

The relationship between the Ca^{2+} current and the intracellular Ca^{2+} concentration at the binding sites on the K_{Ca} channel is dictated by several variables, including the separation between the Ca_v and K_{Ca} channels and the concentrations of fixed and mobile Ca^{2+} buffers, which determine

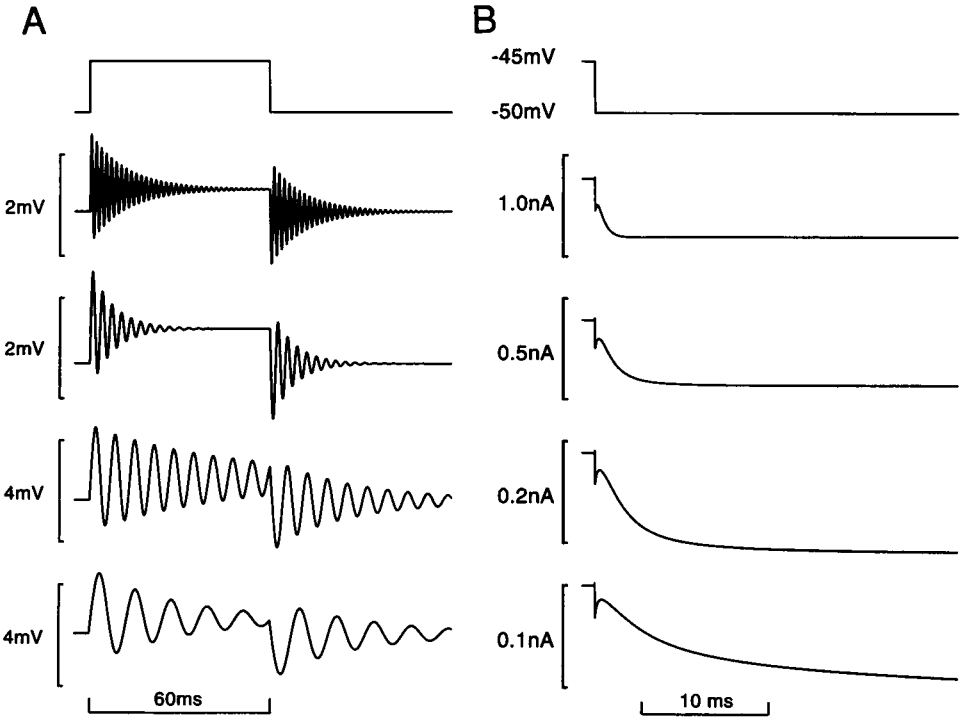

FIGURE 5 (*A*) Current clamp behavior of four model hair cells at row numbers (from top to bottom) of 100, 75, 50, and 25 from apex of cochlea. Resting potential (mV), resonant frequency (Hz), and Q for the four cells are −58, 600, 21; −56, 313, 7.5; −49, 155, 28; −45, 80, 8. The amplitude of the current step in the four cells is (from top to bottom, in pA) 70, 40, 30, and 15. The step was superimposed on standing currents of 400 pA and 70 pA for the top two model cells, respectively. (*B*) Voltage-clamp behavior. Current relaxation at the end of a 5-mV step from −50 to −45 mV. The capacitive current is not shown, and the initial fast transient is due to deactivation of the Ca^{2+} current. Note the slower relaxation in the cells tuned to lower frequencies. This difference was still present if the resting potential rather than −50 mV was used as the holding potential.

the effective diffusion rate of Ca^{2+} (Roberts, 1994; Wu et al., 1995). The values of these variables and their dependence on resonant frequency are largely unknown. They are encapsulated in the reconstruction by the constants S_f and k_R in Eq. 6. In our previous modeling (Wu et al., 1995) it was necessary to make S_f increase with F_o to raise the Ca^{2+} concentration high enough locally to activate the K_{Ca} channel, and in the present scheme, k_R was also allowed to vary. The procedure employed was, for a subset of the locations, to vary S_f and k_R so as to optimize the sharpness of tuning (the Q) and to ensure that the Q was maximized within a few millivolts of the resting potential. This resulted in systematic trends in S_f and k_R, the net effect of which was to raise the internal Ca^{2+} concentration and hence increase the probability of opening, P_{open}, of the K_{Ca} channel high enough at the resting potential to make the ringing behavior clearly visible. At the membrane potential corresponding to the maximum Q, P_{open} for the five channel types fell between about 0.3 and 0.5 of the maximum probability of opening. The relationships between S_f and k_R and the row number, n, were fitted with power functions (plotted in Fig. 7), which were used in the final reconstructions (see Appendix). Although the functions may seem an arbitrary feature of the model, in practice it was difficult, once the channel properties had been specified, to find an alternative pair of parameters, S_f and k_R, that would generate ringing. The change in S_f and k_R with hair cell location would be consistent with gradients in the concentrations of Ca^{2+}

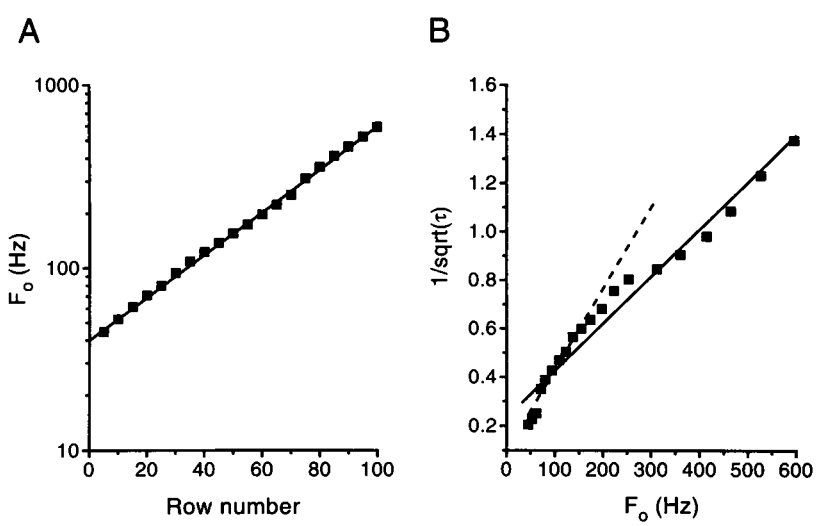

FIGURE 6 (*A*) Frequency map in the turtle cochlea inferred from the resonant frequency of model hair cells in every fifth row. Line is calculated from Eq. 1. The resonant frequency was determined from the frequency of the oscillations in membrane potential at the end of a small depolarizing current step, as in Fig. 5 *A*. (*B*) Variation in the time constant, τ, of the K_{Ca} current obtained by fitting with a single exponential the current relaxations at the end of a 5-mV depolarizing step like those shown in Fig. 5 *B*. $\tau^{-1/2}$ is plotted against the resonant frequency F_o. The continuous line is a fit to the 20 points and the dashed line was used to fit the experimental results in figure 6 *B* of Art and Fettiplace (1987).

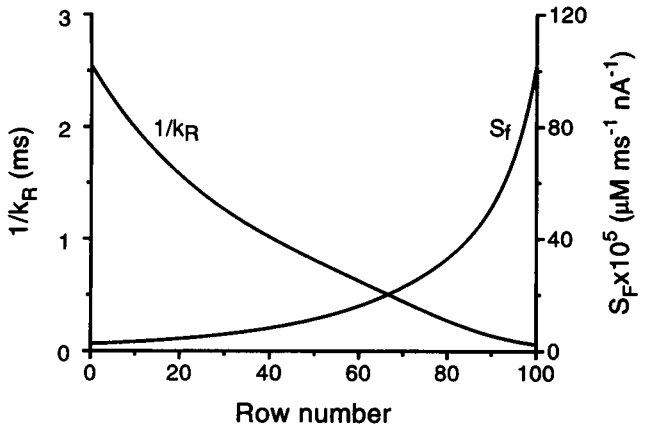

FIGURE 7 Theoretical variations with hair cell location in the two parameters k_R and S_f in Eq. 6. S_f is a scaling factor and k_R is a removal rate constant that together determine the time course and steady level of the Ca^{2+} concentration change at the K_{Ca} channel. These variations were calculated from Eqs. A10 and A11 and are needed to generate high-Q resonance.

pumps and buffers in cells along the cochlea. It should be emphasized that, in a given cell, the value of k_R^{-1} is five to ten times faster than the relaxation rate of the K_{Ca} current, which is presumably limited by conformation changes in the K_{Ca} channels. This contrasts with the model of Ashmore and Attwell (1985), where Ca^{2+} removal was assumed to be rate limiting and held responsible for the K_{Ca} channel kinetics.

Other K_{Ca} channel schemes

The use of only two types of subunit, A and B, is one particular procedure for creating different K_{Ca} channel kinetics. By using A and B subunits as components of a tetrameric channel, it is possible to produce five species of K_{Ca} channel with overlapping distributions. Several other types of scheme for regulating the K_{Ca} channel involving one- or two-channel subunits were considered.

One-channel type

At one extreme, the kinetics could be varied continuously, with the rates of the three critical steps changing according to the fits in Fig. 2 *B*. This is essentially the model considered earlier (Wu et al., 1995), which can generate sharply tuned ringing behavior. Such a model requires that the kinetics of a single-K_{Ca} channel type be modulated over a wide range, perhaps by the regulator molecule, X, the concentration of which varies along the cochlea. X would thus control in a graded fashion the K_{Ca} channel kinetics as well as the numbers of channels.

Two-channel types

The simplest multichannel scheme would be two channel types with different kinetics, whose patterns of expression were inversely related. At one end of the cochlea, only one type of channel would occur, whereas at the other end, only the other type would occur. For all intervening locations the gradation in kinetics would be generated by a mixture of the two types. This could arise if the two subunits, A and B, considered in the original scheme, were unable to hybridize. Such incompatibility occurs between members of the four subfamilies of voltage-gated K^+ channels (Covarrubias et al., 1991; Li et al., 1992). We have found this scheme hard to reconcile with the experimental findings for two major reasons. For intermediate resonant frequencies, the model produces voltage-clamp tail currents with two distinct kinetic components. Different hair cells possess different fractions of these same two components. In contrast, experimental tail currents are well fit by a single time constant that changes systematically. Furthermore, the two components are sufficiently separate kinetically that when they are present in comparable proportions they act to shunt each other and generate a low Q. The problem is especially acute because of the large difference between the two components. Thus the sharpness of tuning could be optimized at the two extremes of the cochlea but not in the middle.

Three-channel types

This scheme is a simpler version of the original, which can be generated by using two subunits, A and B, to construct a dimeric channel. The three forms of channel would then be A_2, AB, and B_2. The distribution of channel types can be predicted in a manner similar to that for the five-channel types, as illustrated in Fig. 4. This model shows a performance intermediate between the two-channel and five-channel schemes. Its defects are less extreme variants of those of the two-channel scheme. In hair cells where two of the components mix, the Q is reduced. For example, in hair cells located at rows 30 to 50, the tuning was very poor, with the Q falling between 1.4 and 2.7. Another problem is that the frequency map was not exponential, and when plotted on log/linear coordinates it had a sigmoidal rather than linear form, thus violating the starting assumption (Eq. 1). It is conceivable that these problems might be alleviated by further optimization (e.g., of the S_f and k_R variables in Eq. 6). We cannot firmly exclude this type of scheme, but its performance was worse than that of the five-channel scheme.

Two-regulator case for K_{Ca} channels

Four different schemes have been considered for generating the diversity in K_{Ca} channel kinetics. As presented, these schemes require regulation in the expression of either one- or two-channel subtypes or constituent subunits. A gradient in the concentration of a single regulator molecule, X, is clearly adequate to control the expression of one subunit and may be extended to two subunits, provided it promotes the expression of one (e.g., B) and inhibits the production of

the other (A). This section shows that opposing gradients in two regulator molecules, which may have certain advantages in terms of signal-to-noise ratio when the concentration of one of the molecules is low, are formally equivalent to the analysis derived for a single regulator molecule.

The derivation of the two-regulator case utilizes the same information as in the single-regulator case. Equations 1 to 12 also hold for the two-regulator case, but the steady-state concentrations at the nth row, $[A]_n^\infty$ and $[B]_n^\infty$, are now controlled by two regulators, $[Y]_n^\infty$ and $[Z]_n^\infty$. Both $[Y]_n^\infty$ and $[Z]_n^\infty$ possess exponential gradients along the cochlea but in opposing directions:

$$[Y]_n^\infty = [Y_o] \cdot e^{-n/\lambda}, \tag{28}$$

$$[Z]_n^\infty = [Z_o] \cdot e^{n/\lambda}, \tag{29}$$

where $[Y_o]$ and $[Z_o]$ are constants. As in the single-regulator case, the relationships between $[A]_n^\infty$ and $[Y]_n^\infty$ and $[B]_n^\infty$ and $[Z]_n^\infty$ are assumed to be power functions:

$$[A]_n^\infty = C_A + \gamma_A \cdot ([Y]_n^\infty)^{m_A}, \tag{30}$$

$$[B]_n^\infty = C_B + \gamma_B \cdot ([Z]_n^\infty)^{m_B}, \tag{31}$$

where C_A, γ_A, m_A, C_B, γ_B, and m_B are unknown parameters. The same boundary conditions, Eqs. 16, 17, and 12, are required to fix the values of these parameters. The relationships between substances A, B, Y, Z and the number of various subtypes of channels can then be constructed:

$$\begin{aligned}[A]_n^\infty &= \omega \cdot e^{n_{min}/4\lambda} \cdot \frac{(e^{n_{max}/4\lambda} - e^{n/4\lambda})}{(e^{n_{max}/4\lambda} - e^{n_{min}/4\lambda})} \\ &= \omega \cdot e^{n_{min}/4\lambda} \cdot \frac{(e^{n_{max}/4\lambda} - \sqrt[4]{[Y_o]/[Y]_n^\infty})}{(e^{n_{max}/4\lambda} - e^{n_{min}/4\lambda})},\end{aligned} \tag{32}$$

$$\begin{aligned}[B]_n^\infty &= \omega \cdot e^{n_{max}/4\lambda} \cdot \frac{(e^{n/4\lambda} - e^{n_{min}/4\lambda})}{(e^{n_{max}/4\lambda} - e^{n_{min}/4\lambda})} \\ &= \omega \cdot e^{n_{max}/4\lambda} \cdot \frac{(\sqrt[4]{[Z]_n^\infty/[Z_o]} - e^{n_{min}/4\lambda})}{(e^{n_{max}/4\lambda} - e^{n_{min}/4\lambda})},\end{aligned} \tag{33}$$

$$\begin{aligned}N_{A_pB_q} &= \frac{(p+q)! \cdot k_1 \cdot k_2 \cdot M_o \cdot V_{cell}}{p! \cdot q! \cdot k_{-1} \cdot k_{-2}} \cdot ([A]_n^\infty)^p \cdot ([B]_n^\infty)^q \\ &= \frac{(p+q)! \cdot a_F \cdot F_o(n_{min})}{p! \cdot q! \cdot (1 - e^{n_{min} - n_{max}/4\lambda})^4} \\ &\quad \cdot (1 - \sqrt[4]{[Y_o]/[Y]_n^\infty} \cdot e^{-n_{max}/4\lambda})^p \\ &\quad \cdot (\sqrt[4]{[Z]_n^\infty/[Z_o]} \cdot e^{-n_{min}/4\lambda} - 1)^q.\end{aligned} \tag{34}$$

The above equations are mathematically equivalent to Eqs. 25–27. Moreover, the frequency and the location at which each type of channel dominates the others are unchanged. Consequently, even though the two regulatory models are significantly different in concept, they can predict the same behavior of the electrical tuning.

From Eqs. 28 and 29 the regulator molecule Z is an increasing function of n, the row number from the apex, and Y is a decreasing function. It is therefore possible to assign one or the other of these molecules as the major regulator of each of the channel variables. For example, the number of inward rectifier channels, $N_{K_{IR}}$, increases with $[Y]_n^\infty$, whereas the number of transducer channels, $N_{C_{MT}}$, which is assumed to be proportional to the number of stereocilia, increases with $[Z]_n^\infty$.

Chick cochlea

Compared to the turtle cochlea, with a 15-fold change of resonant frequency in 100 rows of hair cells, the chick cochlea encodes frequencies from 150 to 4000 Hz over a distance of about 500 rows. Thus the chick cochlea has both a twofold larger frequency range and a greater resolution in terms of rows per octave. The tall chick hair cells also possess electrical tuning (Fuchs et al., 1988) and a complement of membrane channels similar to those found in the turtle (Fuchs, 1992). These include K_{Ca}, K_{IR}, and Ca_V channels, although there is less complete evidence on the existence of gradients in these characteristics (Fuchs and Evans, 1990; Murrow, 1994; Navaratnam et al., 1995). Furthermore, the tuning in the avian cochlea may be a more complex process, involving the cooperation of two types of hair cell (Tanaka and Smith, 1978) and some mechanical tuning of the basilar membrane (Gummer et al., 1987). However, as a first attempt, we shall assume that the model used for the turtle may be extended to the chick, with some modifications. First, a correction was applied to extrapolate from room temperature, 22°C, at which the turtle measurements were made, to the avian body temperature of 39°C, at which the chick frequency map was performed (Manley et al., 1987; Jones and Jones, 1995). The temperature difference results in approximately a sevenfold increase in the rate constants and a doubling of the peak conductances (for justification, see Wu et al., 1995). In addition, a temperature correction was applied to the Ca^{2+} buffering parameters, S_f and k_R, in Eq. 6, the rate constant, k_R, being doubled and the scaling factor, S_f, multiplied by 4. Second, because of the greater frequency resolution, the value for the space constant, λ, in Eq. 1 was increased to 125 rows.

With only these two alterations, the model produced poor tuning, resembling that for the turtle cochlea when only two channel types were allowed (see above). The tuning was improved by adding an extra subunit, C, and arranging for subunits A and B to cover one-half of the cochlea, and B and C to cover the other half, thus effectively producing a pair of turtle cochleas back to back to accommodate the twofold greater frequency range. The three subunits with distributions shown in Fig. 9 *B* combine to form nine K_{Ca} channel types: A_4, A_3B, A_2B_2, AB_3, B_4, B_3C, B_2C_2, BC_3, and C_4. It should be noted that the subunit concentrations could not be specificed by a single regulator molecule, and at least two regulators were needed. The procedure for

deriving the subunit concentrations was similar to that given in the section on two regulators, with the boundary conditions given by

$$[A]^{\infty}_{n_{min}} = [A_o], [B]^{\infty}_{n_{min}} = [C]^{\infty}_{n_{min}} = 0\ \mu M, \text{ for } n = n_{min}, \quad (35)$$

$$[C]^{\infty}_{n_{max}} = [C_o], [A]^{\infty}_{n_{max}} = [B]^{\infty}_{n_{max}} = 0\ \mu M, \text{ for } n = n_{max}, \quad (36)$$

$$[A]^{\infty}_{n_{mid}} = [C]^{\infty}_{n_{mid}} = 0\ \mu M, \qquad \text{for } n = n_{mid}. \quad (37)$$

where rows $n_{min} = 0$, $n_{max} = 500$, and $n_{mid} = 250$. Examples of the ringing evoked by current pulses in a set of model cells are shown in Fig. 8. The records correspond to row numbers and resonant frequencies of 0 (134 Hz), 100 (299 Hz), 200 (530 Hz), 300 (979 Hz), 400 (1827 Hz), and 500 (3993 Hz). The model produces a frequency map (Fig. 9 *A*) in reasonable agreement with both the initial assumption and the experimental measurements (Manley et al., 1987; Jones and Jones, 1995). The maps derived from the two sets of experimental results (see Jones and Jones, 1995) are also given in Fig. 9 *A*.

The quality factor, Q, for the model cells ranged from 3.4 to 24, and the resting potential lay between −50 and −62 mV, both Q and resting potential increasing with resonant frequency. The aspect of the chick model, where cells tuned to higher frequencies possessed more hyperpolarized resting potentials, was also present in the turtle, and had the consequence that, in such cells, the maximum Q occurred at a membrane potential significantly depolarized from rest. Therefore, to measure the resonant frequency at maximum Q, it was necessary to superimpose the current pulse upon a standing inward current (Fig. 8 legend). This defect in the model might be corrected by including in high-frequency cells an inward rectifier current like the I_h described by Holt and Eatock (1995). This is a mixed Na^+/K^+ current, with reversal potential positive to the resting potential, that is activated by hyperpolarization.

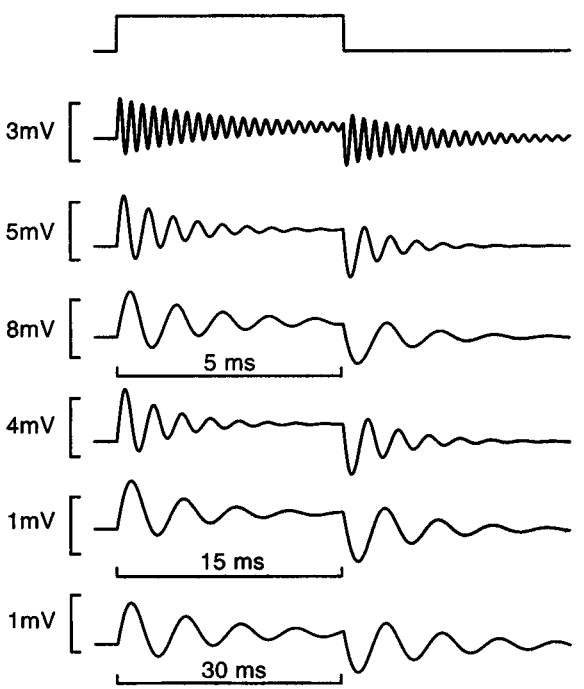

FIGURE 8 Current clamp behavior of six model hair cells in the chick cochlea at row numbers (from top to bottom) of 500, 400, 300, 200, 100, and 0 from the apex. Resting potential (mV), resonant frequency (Hz), and Q for the six cells are −62, 3993, 24; −60, 1827, 6.7; −56, 979, 5.8; −52, 530, 5.3; −50, 299, 3.7; −52, 134, 5.3. The amplitude of the current step was (from top to bottom, in pA): 700, 620, 440, 140, 20, and 10. The step was superimposed on standing currents of 3000 pA and 500 pA for the top two model cells, respectively.

DISCUSSION

Assumptions

We have proposed a model to generate electrical tuning in an array of hair cells over a range of frequencies similar to that found in the turtle and chick cochleas. Two features of the model were an explicit mechanism for altering the K_{Ca} channel kinetics and a set of functions that would enable a gradient in one or two chemicals to regulate the gamut of hair cell properties. The model's main assumptions are i) the form of the frequency map (Eq. 1); ii) the change of K_{Ca} channel numbers with position (Eq. 2); iii) a kinetic scheme for the K_{Ca} channel with a small number of variable rate constants (Eq. 7 and Fig. 2 *B*); and iv) a gradient in the Ca^{2+} buffering and extrusion mechanisms (Eq. 6 and Fig. 7). The first three assumptions are based on evidence gleaned from recordings in isolated turtle hair cells (Art and Fettiplace, 1987; Art et al., 1993, 1995). The fourth assumption was employed as a means of optimizing the tuning. Given the change in Ca^{2+} current along the cochlea, it seems reasonable to assume a parallel change in the processes associated with Ca^{2+} homeostasis, although the use of a power function to describe the gradient is arbitrary. This assumption could be examined by measuring Ca^{2+} turnover in isolated hair cells with a range of resonant frequencies, using methods given by Tucker and Fettiplace (1995). Because the variable parameters, S_f and k_R, in Eq. 6 describe the handling of Ca^{2+} on a millisecond time scale, it seems likely that these partly reflect the cytoplasmic Ca^{2+} buffering capacity (Roberts, 1994), which would be expected to increase with resonant frequency. Recent evidence shows that transcripts for a major hair cell Ca^{2+} buffer, calbindin-D28k, occur at higher concentration in the basal half of the chick cochlea than in the apical half (Navaratnam et al., 1995).

K_{Ca} channel regulation

The K_{Ca} channel has been represented by a kinetic scheme (Eq. 7) that we found to give a reasonable fit to the dwell-time distributions in four channels from hair cells with different resonant frequencies (Wu et al., 1995). However, this scheme does not necessarily depict a realistic model of the channel, and furthermore, the changes in the scheme's

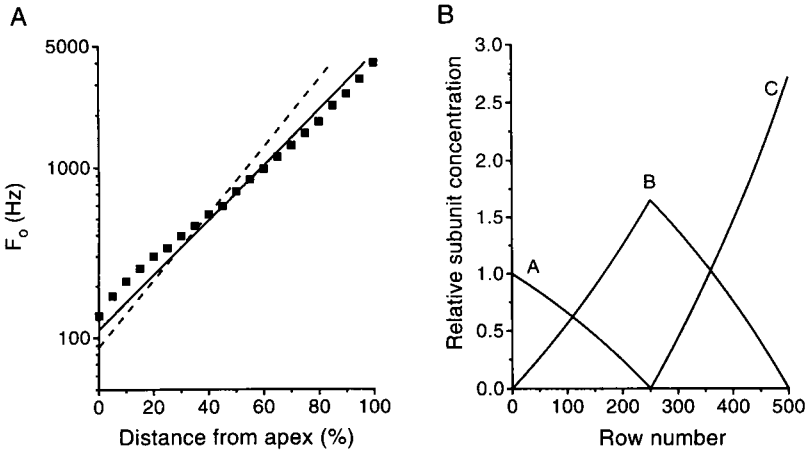

FIGURE 9 (*A*) Theoretical tonotopic map for the chick cochlea deduced from the resonant frequency of model hair cells in every fifth row. The continuous line is the fit to the experimental measurements of Jones and Jones (1995) for stage E19 chick, and the dashed line is the fit to the results of Manley et al. (1987) for stage P2 chick. For fitting parameters see Jones and Jones (1995). Owing to differences in cochlear length between the sets of data, the abscissa is expressed as the percentage distance from the apex. (*B*) Distribution of the three types of K_{Ca} channel subunit, A, B, and C, used to generate the range of resonant frequencies in the chick cochlea.

three rate constants (Fig. 2 *B*) may have no exact physical counterpart and may merely provide a convenient method for quantifying the variations in channel kinetics. Nevertheless, the experiments indicated a systematic trend in the channel's mean open time (Art et al., 1995), as shown in Fig. 2 *A*. The model literally predicts five channel species with distinct kinetics, but no evidence is yet available for such clustering of the channel kinetics. If such groupings exist, the data in Fig. 2 *A* are insufficient to reveal them. However, small experimental differences might easily blur the groupings, especially for the shorter time constants, where the theoretical values are closely spaced. It does seem unlikely that the results in Fig. 2 *A* are derived from two or three discrete channel types, the clustering of which would be more evident: to generate the range of frequencies five or more K_{Ca} channel types may be needed. A particular example of a multichannel model is one where the properties of one K_{Ca} channel protein are modulated, for example, by phosphorylation (Rheinhart et al., 1991) or by association with accessory proteins such as β subunits (Knaus et al., 1994). However, again, the modulator must be capable of generating at least five channel varieties differentially distributed along the cochlea.

Identity of the regulator molecule

Although the source and identity of the morphogen, X, are unknown, several comments can be made about this type of regulatory scheme. First, an exponential gradient in X could arise by diffusion from a continuous source, as might occur if cells at one end of the cochlea were to secrete a gene-regulatory protein during hair cell development. With a single activator molecule, X, the source would be at the base of the cochlea and might define the cochlea's junction with the saccule. There are precedents for gradients in a morphogen controlling tissue differentiation, but the distance over which regulation occurs is usually less than 1 mm (Alberts et al., 1994). The total cochlear length in adult *Trachemys scripta* is 1 mm, but in young turtles the cochlea may be only a third of that (Fettiplace, unpublished observations). The chick attains its full complement of hair cells around E9 when the basilar papilla is about 1 mm long (Tilney et al., 1986), which may still be within the range of action of a single morphogen. It is worth emphasizing that although the channel subunit profiles are shallow (Fig. 4 *A*), incorporation of these subunits into a tetrameric K_{Ca} channel sharpens the boundaries between the different channel species (Fig. 4 *B*). The use of cooperativity may be a general principle for accentuating the response to a concentration gradient in a morphogen.

Interestingly, the mechanism adopted in extrapolating the model from the turtle to the chick with the use of additional subunits (cf. Figs. 4 *A* and 9 *B*) could, in theory, be applied to an even longer cochlea with a greater span of characteristic frequencies. An immediate question then is how the concentration gradients for multiple subunits such as those in Fig. 9 *B* might be established. One strategy could involve the use of a signaling cascade, where the initial gradient in one subunit regulator organizes an opposite gradient in a second regulator; the two regulators then interact to create a local gradient in a third regulator, the process continuing until the distributions in the appropriate number of subunits have been specified. Such sequential positional controls have previously been described in the development of the *Drosophila* embryo (Alberts et al., 1994).

A second point is that the development of the hair cell's disparate properties might be separated in time, with some aspects of the regulation being sequential rather than parallel. This mechanism would not necessarily conflict with our model, because the mature properties might still appear as though they had been independently induced by a single morphogen. As an example, it is known that chick hair cells at E14 possess fully developed voltage-dependent Ca^{2+} channels but only slow voltage-dependent K^+ channels instead of the K_{Ca} channels (Fuchs and Sokolowski, 1990). The adult concentration of K_{Ca} channels is not acquired until later, and it seems possible that the number of these channels synthesized or inserted into the membrane is regulated by a prior gradient in the number of Ca^{2+} channels.

APPENDIX: SUMMARY OF MATHEMATICAL MODEL

Voltage-sensitive Ca^{2+} channel

Ca^{2+} currents in turtle hair cells can be fit by an m^2 relation (Art and Fettiplace, 1987) consistent with the following kinetic scheme for closed (C) and open (O) states:

$$[C \underset{\alpha_m}{\overset{\beta_m}{\rightleftarrows}} O]^2, \tag{A1}$$

with a gating probability, O_m, given by the differential equation

$$\frac{dO_m}{dt} = \beta_m \cdot (1 - O_m) - \alpha_m \cdot O_m, \tag{A2}$$

and rate constants for opening (β_m in s^{-1}) and closing (α_m in s^{-1}) that depend on membrane potential V (in mV):

$$\alpha_m = 5.5 \cdot e^{-V/8.0} + 765, \tag{A3}$$

$$\beta_m = 1.23 \times 10^5 \cdot e^{V/6.2} + 1410. \tag{A4}$$

These values were derived from fits to experimental records giving a half-activation for the conductance at −30 mV, a slope factor of 8.0 mV, and an activation time constant of about 0.3 ms at −50 mV. The probability of opening of the Ca^{2+} channel, p_{Ca}, is then

$$p_{Ca} = (O_m)^2. \tag{A5}$$

The single Ca^{2+} channel current, i_{Ca}, was calculated from the constant field equation

$$i_{Ca} = \frac{P' \cdot \theta \cdot (e^{-\theta} \cdot [Ca^{2+}]_o/[Ca^{2+}]_i - 1)}{e^{-\theta} - 1}, \tag{A6}$$

where $\theta = 2FV/RT \approx 0.08V$. The values of the constant P' (in pA) and the ratio $[Ca^{2+}]_o/[Ca^{2+}]_i$ were adjusted empirically to give a reversal potential of +100 mV and a single-channel current of 0.6 pA at −50 mV (Art et al., 1995). i_{Ca} becomes (in pA)

$$i_{Ca} = \frac{4.94 \times 10^{-5} \cdot \theta \cdot (2981 \cdot e^{-\theta} - 1)}{e^{-\theta} - 1}. \tag{A7}$$

In this equation, $[Ca^{2+}]_o/[Ca^{2+}]_i = 2981$, so with a normal $[Ca^{2+}]_o$ of 2.8 mM, $[Ca^{2+}]_i$ is about 1 μM. The number of Ca^{2+} channels is twice $N_{KCa}(n)$, the number of K_{Ca} channels (Wu et al., 1995), so the total Ca^{2+} current, I_{Ca}, is

$$I_{Ca} = 2 \cdot N_{KCa}(n) \cdot i_{Ca} \cdot p_{Ca}, \tag{A8}$$

and the averaged single Ca^{2+} current, $\bar{i}_{Ca}$, is equal to $i_{Ca} \cdot p_{Ca}$.

Ca^{2+} diffusion and removal process

Diffusion, buffering, and removal of Ca^{2+} are represented by a first-order differential equation, with the concentration, $[Ca^{2+}]$, at the K_{Ca} channel being given by

$$\frac{d[Ca^{2+}]}{dt} = S_f \cdot \bar{i}_{Ca} - k_R \cdot [Ca^{2+}], \tag{A9}$$

where k_R in ms^{-1} is a removal rate constant and S_f (in μM/ms/nA) is a scaling factor that determine the time course and steady level of the Ca^{2+} concentration change. The empirical relationships among S_f, k_R, and regulators are specified as follows:

$$S_f = 1.67 + 1.20 \cdot e^{1.5 \cdot n/\lambda} + 4.88 \times 10^{-8} \cdot e^{7.5 \cdot n/\lambda}, \tag{A10}$$

$$k_R = -0.45 + 0.82 \cdot e^{0.5 \cdot n/\lambda} + 2.82 \times 10^{-4} \cdot e^{4 \cdot n/\lambda}, \tag{A11}$$

where the term $e^{n/\lambda}$ is equivalent to $[X]_n^\infty/[X_o]$ or $[Z]_n^\infty/[Z_o]$ for the single- and two-regulator cases.

Ca^{2+}-activated K channel

The probability p_i^r of the K_{Ca} channel being in a given state i was computed from the kinetic scheme r for the channel at a specified membrane potential, V, and Ca^{2+} concentration, $[Ca^{2+}]$, given by Eq. A9:

$$\frac{dp_i^r}{dt} = \sum_{j=1, j\neq i}^{N} (p_j^r \cdot k_{ji}^r - p_i^r \cdot k_{ij}^r) \quad \text{for } i = 1 \text{ to } N,\ r = 1 \text{ to } 5, \tag{A12}$$

where N is the total number of states (10 for Eq. 7) and is the rate constant from state i to state j of the kinetic scheme r. If there is no transition from i to j, $k_{ij}^r = 0$. Three rate constants from C_{1Ca} to C_{2Ca}, C_{3Ca} to C_{4Ca}, and O_{4Ca} to C_{4Ca} are varied with the relationships according to the position of a hair cell (Wu et al., 1995):

$$k_{C_1 \to C_2}^n = 0.017115 + 0.000572 \cdot e^{2.5n/\lambda}, \tag{A13}$$

$$k_{C_3 \to C_4}^n = 0.018924 + 0.000461 \cdot e^{3n/\lambda}, \tag{A14}$$

$$k_{O_4 \to C_4}^n = -0.370185 + 0.371196 \cdot e^{n/\lambda}, \tag{A15}$$

where k_{ij}^n is the empirical value of the rate constant from state i to j at the nth row. The five positions used to determine the rate constants of the five kinetic schemes are 0 (40.0 Hz), 23 (74.5 Hz), 42 (124.5 Hz), 63 (219.6 Hz), and 100 (596.8 Hz). Equation A15 is modified to avoid negative value at the low-frequency end. The terms $e^{n/\lambda}$ can be replaced by $[X]_n^\infty/[X_o]$ or $[Z]_n^\infty/[Z_o]$ for the single- and two-regulator cases. The probability of opening, $p_{K(Ca)}$, is then

$$p_{KCa}^r = \sum_{i \in \Omega} p_i^r, \tag{A16}$$

where Ω is the set of all open states. The total current I_{KCa} flowing through $N_{KCa}(n)$ channels is

$$I_{KCa} = \sum_{r=1}^{5} [N_{KCa}^r(n) \cdot p_{KCa}^r \cdot i_{KCa}], \tag{A17}$$

where $N_{KCa}^r(n)$ for $r = 1$ to 5 is equal to the number of channels with types A_4, A_3B_1, A_2B_2, A_1B_3, and B_4 at the nth row, respectively. The generalized descriptions of $N_{KCa}^r(n)$ are given by Eqs. 27 and 34 for the single- and two-regulator cases. The unitary current, i_{KCa}, was calculated assuming a linear current-voltage relation,

$$i_{KCa} = (V - E_K) \cdot g_{KCa}, \tag{A18}$$

with a potassium equilibrium potential E_K of −90 mV and a single-channel conductance g_{KCa} of 50 pS (Art et al., 1995).

Inward rectifier K^+ conductance

The inward rectifier was assumed to be a voltage-dependent conductance, G_{KIR}, gated with a time constant τ_{KIR} (1.5 ms) and subject to block at

membrane potentials positive to E_K,

$$\tau_{K_{IR}} \cdot \frac{dG_{K_{IR}}(n)}{dt} + G_{K_{IR}}(n) = \frac{\bar{G}_{K_{IR}}(n)}{1 + 1.03 \cdot e^{(V-E_K)/12.7}}. \quad \text{(A19)}$$

$\bar{G}_{KIR}(n)$ (in nS) is the maximum conductance, which varies inversely with the hair cells' resonant frequency (Goodman and Art, 1996). An exponential function is fitted to describe the relationship between the maximum conductance and the location of a hair cell. The equations for single- and two-regulator cases are described as follows:

$$\bar{G}_{K_{IR}}(n) = -0.885 + 29.480 \cdot e^{-n/\lambda}, \quad \text{(A20)}$$

where $e^{-n/\lambda}$ can be substituted by $[X_o]/[X]_n^\infty$ or $[Y]_n^\infty/[Y_o]$ for the single- and two-regulator cases. The inverse of $[X]_n^\infty/[X_o]$ indicates that X is an inhibitory regulator for $\bar{G}_{K_{IR}}(n)$, whereas Y increases $\bar{G}_{K_{IR}}(n)$. Last, the total inward-rectifier current, $I_{K_{IR}}$, is given by

$$I_{K_{IR}} = (V - E_K) \cdot G_{K_{IR}}(n). \quad \text{(A21)}$$

Concentration of subunit types A and B

The steady-state concentrations of $[A]_n^\infty$ and $[B]_n^\infty$ are determined by Eqs. 25 and 26 for the case of single-regulator, and by mathematically equivalent Eqs. 32 and 33 for the two-regulator case.

Governing equation

For a current-clamp step, $I(t)$, the command current is equal to the sum of the capacitive and ionic currents obtained from Eqs. 5, A8, A17, and A21:

$$I(t) = C \cdot \frac{dV}{dt} + I_{Ca} + I_{K_{Ca}} + I_{K_{IR}} + V \cdot G_L(n), \quad \text{(A22)}$$

where C is the membrane capacitance (12.5 pF). Equation A22 was integrated using a fifth-order Runge-Kutta algorithm (Press et al., 1992).

We should like to thank Miriam Goodman and Genie Jones for helpful comments on the manuscript.

This work was supported by a research grant (5 R01 DC01362) to RF from the National Institutes on Deafness and Other Communication Disorders, National Institutes of Health.

REFERENCES

Adelman, J. P., K.-S. Shen, M. P. Kavanaugh, R. A. Warren, Y.-N. Wu, A. Lagrutta, C. T. Bond, and R. A. North. 1992. Calcium-activated potassium channels expressed from cloned complementary DNAs. *Neuron.* 9:209–216.

Alberts, B., D. Bray, J. Lewis, M. Raff, K. Roberts, and J. D. Watson. 1994. Molecular Biology of the Cell, 3rd ed. Garland Press, New York. 1037–1137.

Art, J. J., and R. Fettiplace. 1987. Variation of membrane properties in hair cells isolated from the turtle cochlea. *J. Physiol. (Lond.).* 385:207–242.

Art, J. J., A. C. Crawford, and R. Fettiplace. 1986. Electrical resonance in membrane currents in turtle cochlear hair cells. *Hear. Res.* 22:31–36.

Art, J. J., R. Fettiplace, and Y.-C. Wu. 1993. The effects of low calcium on the voltage-dependent conductances involved in tuning of turtle hair cells. *J. Physiol. (Lond.).* 470:109–125.

Art, J. J., Y.-C. Wu, and R. Fettiplace. 1995. The calcium-activated potassium channels of turtle hair cells. *J. Gen. Physiol.* 105:49–72.

Ashmore, J. F., and D. Attwell. 1985. Models of electrical tuning in hair cells. *Proc. R. Soc. B.* 226:325–344.

Butler, A., S. Tsunoda, D. McCobb, A. Wei, and L. Salkoff. 1993. mSlo, a complex mouse gene encoding "maxi" calcium-activated potassium channels. *Science.* 261:221–224.

Covarrubias, M., A. Wei, and L. Salkoff. 1991. Shaker, Shal, Shab and Shaw express independent K^+ current systems. *Neuron.* 7:763–773.

Crawford, A. C., and R. Fettiplace. 1980. The frequency selectivity of auditory nerve fibres and hair cells in the cochlear of the turtle. *J. Physiol. (Lond.).* 306:79–125.

Crawford, A. C., and R. Fettiplace. 1981. An electrical tuning mechanism in turtle cochlear hair cells. *J. Physiol. (Lond.).* 312:377–412.

Fettiplace, R. 1987. Electrical tuning of hair cells in the inner ear. *Trends Neurosci.* 10:421–425.

Fuchs, P. A. 1992. Ionic currents in cochlear hair cells. *Prog. Neurobiol.* 39:493–505.

Fuchs, P. A., and M. G. Evans. 1988. Voltage oscillations and ionic conductances in hair cells isolated from the alligator cochlea. *J. Comp. Physiol. A.* 164:151–163.

Fuchs, P. A., and M. G. Evans. 1990. Potassium currents in hair cells isolated from the cochlea of the chick. *J. Physiol. (Lond.).* 429:529–552.

Fuchs, P. A., and B. H. A. Sokolowski. 1990. The acquisition during development of Ca-activated potassium currents by cochlear hair cells of the chick. *Proc. R. Soc. Lond. B.* 241:122–126.

Fuchs, P. A., T. Nagai, and M. G. Evans. 1988. Electrical tuning in hair cells isolated from the chick cochlea. *J. Neurosci.* 8:2460–2467.

Goodman, M. B. 1995. A functional analysis of potassium currents in turtle cochlear hair cells. Ph.D. dissertation. University of Chicago.

Goodman, M. B., and J. J. Art. 1996. Positive feedback by a potassium selective inward rectifier enhances tuning in vertebrate hair cells. *Biophys. J.* In press.

Gummer, A. W., J. W. T. Smolders, and R. Klinke. 1987. Basilar membrane motion in the pigeon measured with the Mössbauer technique. *Hear. Res.* 29:63–92.

Hackney, C. M., R. Fettiplace, and D. N. Furness. 1993. The functional morphology of stereociliary bundles on turtle cochlear hair cells. *Hear. Res.* 69:163–175.

Holt, J. R., and R. A. Eatock. 1995. Inwardly rectifying currents of saccular hair cells from the leopard frog. *J. Neurophysiol.* 73:1484–1502.

Hudspeth, A. J., and R. S. Lewis. 1988a. Kinetic analysis of voltage- and ion-dependent conductances in saccular hair cells of the bullfrog, *Rana catesbeiana. J. Physiol. (Lond.).* 400:237–274.

Hudspeth, A. J., and R. S. Lewis. 1988b. A model for electrical resonance and frequency tuning in saccular hair cells of the bullfrog, *Rana catesbeiana. J. Physiol. (Lond.).* 400:275–297.

Isacoff, E. Y., Y. N. Jan, and L. Y. Jan. 1990. Evidence for the formation of heteromultimeric potassium channels in Xenopus oocytes. *Nature.* 345:530–534.

Jiang, G.-J., M. Zidanic, C. Grigeur, and P. A. Fuchs. 1995. cSlo, a calcium-activated potassium channel gene expressed in the chick's cochlea. *Soc. Neurosci. Abstr.* 21:1326.

Jones, S. M., and T. A. Jones. 1995. The tonotopic map in the embryonic chicken cochlea. *Hear. Res.* 82:149–157.

Knaus, H.-G., K. Folander, M. Garcia-Calvo, M. L. Garcia, G. J. Kaczorowski, M. Smith, and R. Swanson. 1994. Primary sequence and immunological characterization of β-subunit of high-conductance Ca^{2+}-activated K^+ channel from smooth muscle. *J. Biol. Chem.* 269: 17274–17278.

Li, M., Y. N. Jan, and L. Y. Jan. 1992. Specification of subunit assembly by the hydrophilic amino-terminal domain of the Shaker potassium channel. *Science.* 257:1225–1230.

MacKinnon, R. 1991. Determination of the subunit stoichiometry of a voltage-activated potassium channel. *Nature.* 350:232–235.

Manley, G. A., J. Brix, and A. Kaiser. 1987. Developmental stability of the tonotopic organization of the chick's basilar papilla. *Science.* 237: 655–656.

McManus, O. B., and K. L. Magleby. 1991. Accounting for the Ca^{2+}-dependent kinetics of single large-conductance Ca^{2+}-activated K^+ channels in rat skeletal muscle. *J. Physiol. (Lond.).* 443:739–777.

Murrow, B. W. 1994. Position-dependent expression of potassium currents by chick cochlear hair cells. *J. Physiol. (Lond.).* 480:247–259.

Navaratnam, D. S., L. Escobar, M. Covarrubias, and J. C. Oberholtzer. 1995. Permeation properties and differential expression across the auditory receptor epithelium of an inward rectifier K^+ channel cloned from the chick inner ear. *J. Biol. Chem.* 270:19238–19245.

Oberholtzer, J. C., C. Buettiger, M. C. Summers, and F. M. Matchinsky. 1988. The 28-kDa calbindin-D is a major calcium-binding protein in the basilar papilla of the chick. *Biochemistry.* 85:3387–3390.

Pickles, J. O., and D. P. Corey. 1992. Mechanoelectrical transduction by hair cells. *Trends Neurosci.* 15:254–258.

Pitchford, S., and J. F. Ashmore. 1987. An electrical resonance in hair cells of the amphibian papilla of the frog *Rana temporaria. Hear. Res.* 27:75–83.

Press, W. H., S. A. Teukolsky, W. T. Vetterling, and B. R. Flannery. 1992. Numerical Recipes in C. The Art of Scientific Programming. Cambridge University Press, Cambridge, England. 710–722.

Rheinhart, P. H., S. Chung, B. L. Martin, D. L. Brautigan, and I. B. Levitan. 1991. Modulation of calcium-activated potassium channels from rat brain by protein kinase A and phosphatase 2A. *J. Neurosci.* 11:1627–1635.

Roberts, W. M. 1994. Localization of calcium signals by a mobile calcium buffer in frog saccular hair cells. *J. Neurosci.* 14:3246–3262.

Roberts, W. M., R. A. Jacobs, and A. J. Hudspeth. 1990. Colocalization of ion channels involved in frequency selectivity and synaptic transmission in presynaptic active zones of hair cells. *J. Neurosci.* 10: 3664–3684.

Sackmann, B., and G. Trube. 1984. Conductance properties of single inwardly rectifying potassium channels in ventricular cells from guinea-pig heart. *J. Physiol. (Lond.).* 347:641–657.

Sugihara, I., and T. Furukawa. 1989. Morphological and functional aspects of two different types of hair cells in the goldfish sacculus. *J. Neurophysiol.* 62:1330–1343.

Tanaka, K., and C. A. Smith. 1978. Structure of the chicken's inner ear: SEM and TEM study. *Am. J. Anat.* 153:251–272.

Tilney, L. G., and J. C. Saunders. 1983. Actin filaments, stereocilia, and hair cells of the bird cochlea. I. Length, number, width, and distribution of stereocilia of each hair cell are related to the position of the hair cell on the cochlea. *J. Cell Biol.* 96:807–821.

Tilney, L. G., M. S. Tilney, J. C. Saunders, and D. J. Derosier. 1986. Actin filaments, stereocilia, and hair cells of the bird cochlea. III. The development and differentiation of hair cells and stereocilia. *Dev. Biol.* 116:100–118.

Tseng-Crank, J., C. D. Foster, J. D. Krause, R. Mertz, N. Godinot, T. J. DiChiara, and P. H. Rheinhart. 1994. Cloning, expression and distribution of functionally distinct Ca^{2+}-activated K^+ channel isoforms from human brain. *Neuron.* 13:1315–1330.

Tucker, T., and R. Fettiplace. 1995. Confocal imaging of calcium microdomains and calcium extrusion in turtle hair cells. *Neuron.* 15:1323–1335.

Wu, Y.-C., J. J. Art, M. B. Goodman, and R. Fettiplace. 1995. A kinetic description of the calcium-activated potassium channel and its application to electrical tuning of hair cells. *Prog. Biophys. Mol. Biol.* 63: 131–158.